Antibiotic overproduction in Streptomyces coelicolor A3(2) mediated by phosphofructokinase deletion

Borodina, Irina; Siebring, Jeroen; Zhang, Jie; Smith, Colin P.; van Keulen, Geertje; Dijkhuizen, Lubbert; Nielsen, Jens

Published in:
The Journal of Biological Chemistry

DOI:
10.1074/jbc.M803105200

Publication date:
2008

THE JOURNAL OF BIOLOGICAL CHEMISTRY VOL. 283, NO. 37, pp. 25186–25199, September 12, 2008

Antibiotic Overproduction in *Streptomyces coelicolor* A3(2) Mediated by Phosphofructokinase Deletion*[S]

Received for publication, April 23, 2008, and in revised form, June 16, 2008 Published, JBC Papers in Press, July 7, 2008, DOI 10.1074/jbc.M803105200

Irina Borodina[‡1,2], Jeroen Siebring[§1], Jie Zhang[‡], Colin P. Smith[¶], Geertje van Keulen[‖], Lubbert Dijkhuizen[§], and Jens Nielsen[‡3]

From the [‡]Center for Microbial Biotechnology, BioCentrum-DTU, Technical University of Denmark, 2800 Kongens Lyngby, Denmark, the [§]Department of Microbiology, Groningen Biotechnology and Biomolecular Sciences Institute, University of Groningen, P. O. Box 14, 9750 AA, Haren, The Netherlands, [¶]Functional Genomics Laboratory, Faculty of Health and Medical Sciences, University of Surrey, Guildford, Surrey GU2 7XH, United Kingdom, and [‖]Biological Sciences, School of the Environment and Society, Swansea University, Swansea SA2 8PP, United Kingdom

Streptomycetes are exploited for production of a wide range of secondary metabolites, and there is much interest in enhancing the level of production of these metabolites. Secondary metabolites are synthesized in dedicated biosynthetic routes, but precursors and co-factors are derived from the primary metabolism. High level production of antibiotics in streptomycetes therefore requires engineering of the primary metabolism. Here we demonstrate this by targeting a key enzyme in glycolysis, phosphofructokinase, leading to improved antibiotic production in *Streptomyces coelicolor* A3(2). Deletion of *pfkA2* (SCO5426), one of three annotated *pfkA* homologues in *S. coelicolor* A3(2), resulted in a higher production of the pigmented antibiotics actinorhodin and undecylprodigiosin. The *pfkA2* deletion strain had an increased carbon flux through the pentose phosphate pathway, as measured by ^{13}C metabolic flux analysis, establishing the ATP-dependent PfkA2 as a key player in determining the carbon flux distribution. The increased pentose phosphate pathway flux appeared largely because of accumulation of glucose 6-phosphate and fructose 6-phosphate, as experimentally observed in the mutant strain. Through genome-scale metabolic model simulations, we predicted that decreased phosphofructokinase activity leads to an increase in pentose phosphate pathway flux and in flux to pigmented antibiotics and pyruvate. Integrated analysis of gene expression data using a genome-scale metabolic model further revealed transcriptional changes in genes encoding redox co-factor-dependent enzymes as well as those encoding pentose phosphate pathway enzymes and enzymes involved in storage carbohydrate biosynthesis.

Streptomyces are well known for their production of biologically active secondary metabolites, with almost two-thirds of all known natural antibiotics being produced by *Streptomyces*. The best genetically characterized strain is *Streptomyces coelicolor* A3(2), which produces pigmented antibiotics and has become the preferred model organism in *Streptomyces* research.

Secondary metabolites are generally synthesized in dedicated biosynthetic pathways, but these are linked to the primary metabolism through the use of specific precursors and various cofactors. Although still largely unclear, the link between primary and secondary metabolism has been repeatedly observed (1–3). Thus, deletion of the glyceraldehyde 3-phosphate dehydrogenase encoding gene *gap1* improved clavulanic acid production in *Streptomyces clavuligerus* because of increased supply of precursor glyceraldehyde 3-phosphate (4). Furthermore, overexpression of acetyl-CoA carboxylase *acc* in *S. coelicolor* improved the yield of actinorhodin, which uses the Acc product, malonyl-CoA, as a precursor for actinorhodin biosynthesis (5). In another study deletion of important tricarboxylic acid cycle genes, such as citrate synthase (*citA*) or aconitase (*acoA*) in *S. coelicolor*, resulted in glutamate auxotrophy, overproduction of organic acids, as well as changes in secondary metabolite production and morphological differentiation (6, 7). Polyphosphate kinase (*ppk*) gene inactivation in *Streptomyces lividans* was also shown to have an effect on secondary metabolite production as it resulted in accumulation of polyphosphates and activation of actinorhodin production, which is normally silenced in this species (8–10).

To further evaluate the link between primary and secondary metabolism, we decided to study the effect of phosphofructokinase (Pfk)[4] deletion on secondary metabolism in *S. coelicolor*. Pfk is a highly regulated enzyme in the conserved Embden-Meyerhof-Parnas pathway (EMP or glycolysis) catalyzing the phosphoryl transfer to the first position of the substrate fructose 6-phosphate (fructose-6-P). The enzyme generally employs ATP as the source of the phosphoryl group and is

* This work was sponsored in part by European Union 6FP ActinoGEN Project (Contract LSHM-CT-2004-005224). The costs of publication of this article were defrayed in part by the payment of page charges. This article must therefore be hereby marked "*advertisement*" in accordance with 18 U.S.C. Section 1734 solely to indicate this fact.

[S] The on-line version of this article (available at http://www.jbc.org) contains supplemental Figs. S1–S6.

[1] Both authors contributed equally to this work.

[2] Supported by Ph.D. scholarship from Technical University of Denmark.

[3] To whom correspondence should be addressed. Tel.: 45-45252696; Fax: 45-45884148; E-mail: jn@biocentrum.dtu.dk.

[4] The abbreviations used are: Pfk, phosphofructokinase; TES, 2-{[2-hydroxy-1,1-bis(hydroxymethyl)ethyl]amino}ethanesulfonic acid; Tricine, *N*-[2-hydroxy-1,1-bis(hydroxymethyl)ethyl]glycine; MES, 2-(*N*-morpholino)ethanesulfonic acid; HPLC, high pressure liquid chromatography; RT, reverse transcription; qRT, quantitative RT; ACT, actinorhodin; RED, undecylprodigiosin; EMP, Embden-Meyerhof-Parnas pathway; G6PDH, glucose-6-phosphate 1-dehydrogenase; SFL, summed fractional labeling; PPP, pentose phosphate pathway.

TABLE 1

Alignment of N-terminal sequences of all three *S. coelicolor* PfkA isoenzymes and the N-terminal sequence of the previously purified *S. coelicolor* ATP-dependent PfkA protein

Lowercase letters indicate tentatively assigned amino acids; X indicates an unidentified residue; # indicates N-terminal sequence of sequence of the previously purified *S. coelicolor* ATP-dependent PfkA protein, as determined by Alves *et al.* (15); * indicates positions which have a single, fully conserved residue.

(SCO2119) PfkA1	MKVGVLTGGGDCPGLNAVIRAVVRKGVQEYGYDFTGFRDGWRGPLEGDTVPLDIPAVRGI
N-terminus#	MRIGVLTAGGDXPGLNAVIXSVVXXAVD----------
(SCO5426) PfkA2	MRIGVLTAGGDCPGLNAVIRSVVHRAVDNYGDEVIGFEDGYAGLLDGRYRALDLNAVSGI
(SCO1214) PfkA3	MRIGVLTSGGDCPGLNAVIRSVVHRAVVDHGDEVIGFRDGWKGLLECDYLKLDLDAVGGI
	* **** *** ******* ** *

allosterically regulated, usually by a number of effectors. The reaction catalyzed by ATP-dependent Pfks is irreversible, and therefore the six-carbon sugars are confined to the subsequent glycolytic reactions once they passed the Pfk catalyzed step. Besides going to the EMP, glucose 6-phosphate (glucose-6-P) can also enter either the pentose phosphate pathway (PPP) or serve as a precursor for carbohydrate polymer biosynthesis. Alteration of the committing phosphofructokinase activity might influence the flux distribution at the glucose-6-P node. Therefore, Pfk is a high profile target for altering metabolic fluxes in the cell.

The full genome sequence of *S. coelicolor* A3(2) (11) revealed the presence of three highly similar family A-type *pfk* genes (*pfkA*), SCO2119, SCO5426, and SCO1214, with 56–72% identity and 69–82% similarity at the amino acid level. This number of copies is large when compared with closely related, less developmentally complex actinomycetes like *Mycobacterium tuberculosis* (12, 13) and *Corynebacterium glutamicum* (14), which both contain only one *pfkA* gene. The biological reason for the presence of multiple copies of primary metabolic genes such as *pfk* is not known, and there is little information available about the regulation of primary metabolic isoenzymes in *S. coelicolor*. For instance, it is not known whether expression of various isoenzymes is dependent on the developmental phase of a colony or whether the isoenzymes convey different kinetics.

Previously, an. *coelicolor* PfkA enzyme had been purified and characterized as described by Alves *et al.* (15). This ATP-dependent, allosterically controlled enzyme was linked to the *pfkA1* gene (SCO2119). However, inspection of the original N-terminal sequence of the protein purified in that study revealed that the N-terminal sequence does not exactly fit that predicted for PfkA1 but has an identical match to the PfkA2 (SCO5426) enzyme N terminus (Table 1). In this study, we also report that PfkA2 is the only isoenzyme with detectable Pfk activity in *S. coelicolor* extracts, which further confirms that the enzyme studied by Alves *et al.* is indeed PfkA2 (15).[5]

In this study we show that the deletion of *pfkA2* drastically increases pigmented secondary metabolite production in *S. coelicolor*. For this reason we studied the effect of *pfkA2* deletion on intracellular carbon fluxes, metabolite levels, gene expression, and secondary metabolite production to gain more insight in flux distribution and the link between the fluxes in the primary metabolism and secondary metabolism.

[5] A. M. da Costa Rodrigues Alves, personal communication.

EXPERIMENTAL PROCEDURES

Alignment—The alignment of N-terminal amino acid sequences of *S. coelicolor* PfkA isoenzymes, including the PfkA N terminus as determined by Alves *et al.* (15), was performed using ClustalX (16).

Strains—The *S. coelicolor* M145 (SCP1−, SCP2−) strain used for construction of the *pfkA* single gene deletions was kindly supplied by Matthias Redenbach. The ordered cosmid library made from this strain (17) was used in the *S. coelicolor* genome sequencing project (11). Later genotyping of the strain indicated a possible duplication of 20 genes (SCO4672–4695) mostly coding for proteins of unknown function. No gene was found under-represented in this strain. The reference strain used for metabolic flux analysis was *S. coelicolor* M145, which was a gift from Mervyn Bibb, John Innes Centre, UK. To ensure that the unintended duplication in the Redenbach supplied parental strain did not influence the observed phenotype, we also have deleted *pfkA2* in the reference M145 strain. No morphological differences between M145 and the Redenbach strain, or between the *pfkA2* mutants thereof, were observed on plates or in liquid complex medium. Ten genes from the duplicated region, most of them assigned as hypothetical proteins, were found to be overexpressed in the Redenbach Δ*pfkA2* mutant as compared with the reference M145.

The single gene deletion mutants Δ*pfkA1*, Δ*pfkA2*, and Δ*pfkA3* were constructed by λ-mediated recombination in *Escherichia coli* according to the REDIRECT protocol (18). The REDIRECT strategy is based on replacement of a chromosomal sequence within an *S. coelicolor* cosmid (17) by a selectable marker. This marker is PCR-generated using primers with 39-nucleotide homology extensions. These homology extensions are designed to match the immediate flanking regions of the genes targeted allowing stable in-frame, full-length gene replacements.

The *pfkA1* gene was fully replaced with a viomycin resistance cassette, which was amplified from plasmid pIJ780. The *pfkA2* and *pfkA3* genes were replaced by an apramycin resistance cassette generated by PCR from plasmid pIJ773. The primers used in this process are listed in Table 2. The strains were maintained on master plates of mannitol soy flour (MS) agar (19) containing 50 μg/ml apramycin/viomycin for the mutants. The spores from the master plates were streaked onto fresh MS plates, from which spores were harvested to make dense spore plates. The dense spore plates provided inocula for further studies.

TABLE 2

Nucleotide sequence of primers used for λRED-mediated deletion of the *pfkA* genes, of primers used for amplifying internal *pfkA* fragments in RT-PCR, and of primers used for qRT-PCR

The universal 5′ and 3′ ends of the disruption cassette for the gene replacements are underlined.

REDIRECT primers	sequence (5′ – 3′)
pfkA1 forward	GGCCTCAACCACCCACCCTGGCAAAGGGGTTGTGCGATGATTCCGGGGATCCGTCGACC
pfkA1 reverse	ACCGCCGTCGCCGGTCAGCGGCCGTTCCGCCGGACGTCATGTAGGCTGGAGCTGCTTC
pfkA2 forward	TCACCGGTGTCAACAGCGAGCAGGAGACACAGCACGATGATTCCGGGGATCCGTCGACC
pfkA2 reverse	TGGACGGCGGTCGAGAGGCACCCCTAGAGGGGAGGCCTATGTAGGCTGGAGCTGCTTC
pfkA3 forward	CCGGACCCGTGCCACGTTGAGAAGGTATTTCGGGCTATGATTCCGGGGATCCGTCGACC
pfkA3 reverse	GCGAATCACCTCAAGGCCCGAGCTCCGACCGGCAGGTCATGTAGGCTGGAGCTGCTTC
RT primers	**sequence (5′ – 3′)**
pfkA1 forward	GACGGCATCCGGCGCATCAA
pfkA1 reverse	TCTGCTTGGCCAGCCATTCG
pfkA2 forward	GCGAGGCCTGCGAGAACGCG
pfkA2 reverse	AGCGCGGTGCCGATGCCCTG
pfkA3 forward	GGACGGCGTGGAGCGGGCCC
pfkA3 reverse	AGCTGGCGGGCGATCCCGGC
16S forward	CCGCAGCTAACGCATTAAGT
16S reverse	TTGTACCGGCCATTGTAGCA
qRT primers	**sequence (5′ – 3′)**
hrdB forward	CATGCGCTTCGGACTCA
hrdB reverse	ACTCGATCTGGCGGATG
actII-4 forward	GACGCGGGACTGGATCTCT
actII-4 reverse	TGCGCGATATTGCTTTCG
actIII forward	GCGAGCACTACTCGGACATCT
actIII reverse	TCGGACGGCTGCACGTA
redD forward	TCATGGGAGTGCGGAGAAC
redD reverse	CATCCCCCGAAGTTGTACAG
redQ forward	CTGGAGATGGACTCGCTGTTC
redQ reverse	GCGTCGTCGCTGATCTTCA

Batch Cultivations for Metabolic Flux Analysis and Transcription Analysis—Batch cultivations were performed in fermentors with 1 liter working volume (Applikon Biotechnology) at 30 °C, pH 6.8–7.0, 800 rpm agitation rate, and a 1 volume per volume per min aeration rate. The fermentors were equipped with a cooled condenser to avoid evaporation from the medium. pH was controlled by automatic addition of 1 N NaOH. The aeration rate was adjusted after every sampling to compensate for working volume reduction. The concentrations of CO_2 and O_2 were monitored by an acoustic gas analyzer (model number 1311, Bruël & Kjær).

The defined minimal medium was limited in phosphate and contained 3 mM NaH_2PO_4, 100 mM NH_4Cl, 10 mM KCl, 2 mM Na_2SO_4, 2 mM citric acid as chelating agent, 1.25 mM $MgCl_2$, 0.25 mM $CaCl_2$, as well as the following per liter: 20 g of glucose, 5 ml of trace elements solution (20 mM $FeCl_3$, 10 mM $CuCl_2$, 50 mM $ZnCl_2$, 10 mM $MnCl_2$, 0.02 mM Na_2MoO_4, 20 mM $CoCl_2$, 10 mM H_3BO_4), 1 ml of vitamins solution (0.05 g of biotin, 1 g of calcium pantothenate, 1 g of nicotinic acid, 25 g of myo-inositol, 1 g of thiamine-HCl, 1 g of pyridoxine-HCl, and 0.2 g of *para*-aminobenzoic acid/liter), and 100 μl of organic antifoam 204 (Sigma). All components, except glucose and vitamins, were added to the MilliQ water (Millipore) in the fermentor and autoclaved at 121 °C for 40 min. Glucose and vitamins were added after autoclaving, and pH adjustment was by sterile filtration. 30% of the added glucose for the labeled cultivations consisted of [1-^{13}C]glucose (Omicron Biochemicals).

The inoculum for each fermentor was prepared as follows: spores from one dense spore plate were harvested with 2 ml of 20% sterile glycerol, filtered through glass fiber wool to remove mycelial fragments, and inoculated into a 500-ml volume baffled shake flask with 50 ml of 2×YT medium (19) and 30 glass beads (3 mm diameter). The culture was incubated at 30 °C and 150 rpm agitation for 12 h, centrifuged at 3,000 × *g* for 5 min, resuspended in 3–5 ml of residual liquid, and immediately inoculated into a fermentor.

Analysis of Biomass Dry Weight—Throughout cultivation 12-ml samples were taken. Of these samples, 8 ml was filtered through pre-dried Supor®-450 membrane filters (0.45 μm pore, Pall Corp.). The filtrate was collected in a pre-cooled tube and kept at −20 °C until extracellular metabolite analysis. The cells were washed twice with 0.9% sodium chloride and dried in

a microwave oven at 150 watts for 20 min, after which the dry weight of the biomass was calculated. The remaining 4 ml of the sample was divided into 2 × 2-ml portions and kept at −20 °C for antibiotic analysis.

Shake Flask Cultivations for Analysis of Antibiotics, Intracellular Sugar Phosphates, and Carbohydrates—The defined minimal medium for the shake flask cultivation was the same as described for the batch cultivations, but contained 40 g per liter of glucose instead of 20 g per liter, and was supplemented with 50 mM MES for buffering purposes. The pH of the medium was adjusted to 6.8 before autoclaving. The cultivations were performed in 500-ml baffled shake flasks with 50 ml of defined medium and 30 glass beads (3 mm diameter). The cultures were kept at 30 °C on a shaking table with an agitation speed of 150 rpm. The inoculum for shake flasks was prepared in the same way as for the fermentors, except for the centrifugation step. Preculture (2.5 ml) was added directly to each shake flask (5% v/v).

Shake Flask Cultivations for Antibiotic Phenotyping in Complex Medium—*Streptomyces* strains used were grown under standard conditions in 200 ml of R2YE medium (19). The 1-liter flasks were inoculated with 10^6 spores per ml of medium. Spores were pregerminated for 15 min at 50 °C in TY medium (19) and spun down (15 min, 16,100 × *g*). Most of the supernatant was removed before inoculation. The cultures were grown in 1-liter shake flasks equipped with stainless steel spirals at 30 °C while shaken at 200 rpm.

Actinorhodin (ACT) and Undecylprodigiosin (RED) Quantifications—To extract actinorhodin, 2 ml of 3 N KOH was added to a 2-ml sample, vortexed, and left shaking overnight at 2 °C. The suspensions were centrifuged at 4,000 × *g* for 10 min, and the absorbance of the supernatant was measured at 640 nm. The actinorhodin concentration was calculated based on an extinction coefficient of 25,320 M^{-1} cm^{-1} (20). Undecylprodigiosin was extracted in the same manner but with methanol acidified to pH 1.5 with HCl in a tube with 0.25–0.5 mm (diameter) glass beads. The extinction coefficient of undecylprodigiosin used was 100,500 M^{-1} cm^{-1} at 530 nm (21).

Analysis of Extracellular Metabolites—A range of extracellular metabolites, including glucose, was analyzed by HPLC using an Aminex HPX-87H column (Bio-Rad). The operating temperature was 60 °C. Separation was achieved using 5 mM H_2SO_4 at a flow rate of 0.6 ml/min. The HPLC was equipped with a Waters 410 differential refractometer (Millipore) and a tunable absorbance detector set at 210 nm (Waters 486, Millipore). Glucose, glycerol, succinate, and ethanol were quantified using a refractometer, and acetate and pyruvate were quantified by UV absorbance. A calibration curve was made using six different metabolite concentrations.

Analysis of Intracellular Sugar Phosphate Concentrations—Cells from triplicate shake flask cultures were quenched in cold methanol and then extracted with chloroform, pH 7, according to a slightly modified method from de Koning and van Dam (22). Cell culture (10 ml) was used to determine biomass dry weight to calculate the sugar phosphate portion per g dry weight. Cell suspension (5 ml) was sprayed into 20 ml of 60% (v/v) methanol buffered with 12.5 mM Tricine, pH 7.4, and kept in a −40 °C ethanol bath. The cells were centrifuged for 5 min at 4,000 × *g* at −20 °C. The supernatant was collected and kept at −80 °C until further analysis. Pure methanol (2.5 ml) was added to the cell pellet, after which the tube was immersed in liquid nitrogen and stored at −80 °C. The extraction was performed by shaking the tubes at −20 °C overnight at 300 rpm after addition of 5 ml of chloroform, 2 ml of buffer (3 mM Tricine, 3 mM EDTA, pH 7.0), and glass beads 0.25–0.5 mm (diameter). The mixture was centrifuged at 1,200 × *g* for 12 min at −20 °C, and the upper phase was collected. Pure methanol (2 ml) was added to the remaining chloroform, and cells were vortexed, separated by centrifugation, and pooled with the first portion of the extract. The extract and the quenching liquid were freeze-dried, and the solid matter was redissolved in 1 ml of MilliQ water.

Glucose 6-phosphate (glucose-6-P) and fructose 6-phosphate (fructose-6-P) were analyzed in an enzymatic assay with glucose 6-phosphate 1-dehydrogenase (G6PDH) and phosphoglucose isomerase by fluorimetric measurement of NADPH formation on a luminescence spectrometer LS50B (PerkinElmer Life Sciences) set at 340 nm for excitation and 456 nm for emission. The reaction was carried out at room temperature in 250 mM triethanolamine buffer with 0.025 mM $NADP^+$. The sample was added to the buffer, and the base-line absorbance was measured after which 1 unit of G6PDH was added per ml. The increase in absorbance was measured after 5–7 min. The increase in absorbance, and thus NADPH, is proportional to the conversion of glucose-6-P. The additional increase in absorbance after addition of phosphoglucose isomerase corresponds to the amount of fructose-6-P converted.

Glucose-6-P and fructose-6-P amounts were calculated from the calibration curves, which were linear in the 0 to 10.5 nM range. The samples fell within the range of the calibration curve. Some of the samples were measured a few times to determine the measurement error, which was not higher than 5%.

Measurement of Carbohydrate Content—The samples for measurement of carbohydrate content were collected during the stationary phase when the triplicate shake flask cultures became red indicating undecylprodigiosin production. Samples taken (5–10 ml) were centrifuged at 10,000 × *g* for 10 min, washed twice with distilled water, and freeze-dried. 5 mg of dried sample was then dispersed in 1 ml of distilled water. To this mixture 2 ml of 0.5% anthrone in 70% sulfuric acid was added (23). The samples were boiled in a water bath for 20 min and cooled to room temperature, and absorbance was measured at 625 nm and compared with a glucose standard curve.

Measurement of Amino Acid Labeling and Estimation of Metabolic Fluxes—For the labeled cultivations additional samples of 5–10 ml were withdrawn. The biomass was centrifuged at 10,000 × *g* for 5 min, washed twice with cold 0.9% NaCl, and kept at −20 °C until further analysis. The biomass was hydrolyzed with 6 N HCl at 105 °C and then derivatized as described in Christensen and Nielsen (24). The labeling of amino acid fragments was measured by gas chromatography coupled to mass spectrometry (24). The labeling of each fragment was expressed as summed fractional labeling (SFL) determined by Equation 1,

$$SFL = \frac{i_0 \cdot 0 + i_1 \cdot 1 + i_2 \cdot 2 + \ldots + i_n \cdot n}{i_0 + i_1 + i_2 + \ldots + i_n} \quad \text{(Eq. 1)}$$

where i_n is the peak intensity of mass isotopomer with n ^{13}C atoms. The data were corrected for natural isotope abundance before usage (24).

The labeling data together with growth parameters and cellular composition were used to calculate fluxes by an algorithm from Wiechert (25) implemented in an in-house software package based on Matlab (The MathWorks). The cellular composition was taken from Borodina *et al.* (26), except for protein composition, which was specifically determined for *S. coelicolor* cultivations on a defined minimal medium (27) (supplemental Fig. S1).

Diamide Sensitivity Assays—Diamide sensitivity assays were performed as described previously (3, 28). Halo surfaces were determined after 48 h of incubation at 30 °C.

Sampling for Microarray Analysis and RNA Isolation—The samples for gene expression analysis were taken during the exponential growth phase, when the carbon dioxide concentration in the outlet gas was 0.1%, corresponding to ~2 g/liter of dry weight biomass. Samples of 20 ml were withdrawn quickly and sprayed into 50-ml falcon tubes filled with crushed ice resulting in almost immediate cooling down to 0–2 °C. The mixture was shaken and centrifuged at 4,000 × *g* for 1 min. The supernatant was decanted, and the cells were immersed in liquid nitrogen and then stored at −80 °C until RNA extraction. The total time spent on the sampling procedure did not exceed 2 min.

Total RNA extraction was performed with an RNeasy kit (Qiagen) using a FastPrep FP120 (3 × 40 s; Qbiogene) for breaking the cells. After the removal of cellular debris additional steps were performed as follows: two rounds of phenol:chloroform:isoamyl alcohol, pH 8, extraction, and 1 round of chloroform extraction. The rest of the procedure was according to the manufacturer's instructions. The total RNA was subjected to DNase digestion and then concentrated from the reaction solution using an RNeasy CleanUp kit (Qiagen). The quality of RNA was assessed on a Bioanalyzer (Agilent) to ensure that no degradation of 23 S rRNA or 16 S rRNA had occurred.

Microarray Analysis—The arrays were spotted oligonucleotide arrays (University of Surrey fabricated oligonucleotide (50 mer) microarrays), containing duplicate spots of probes for 7623 *S. coelicolor* genes. Each probe was 50 nucleotides long and was designed for minimal cross-hybridization with other genes.

The RNA samples were labeled and hybridized to the arrays according to the procedure described on line. The design included three biological replicates for the reference strain and two biological replicates for the Δ*pfkA2* mutant as well as dye swaps. Only two biological replicates were analyzed in case of Δ*pfkA2* because one of the RNA preparations did not pass the quality control. We applied loop design (29), where samples were compared directly to each other without a common reference (supplemental Fig. S2).

Array Image Analysis and Data Normalization—The arrays were scanned using an Affymetrix 428 laser scanner (Affymetrix). Image analyses were carried out using BlueFuse software (BlueGnome Ltd.), which allows automatic grid alignment, spot boundary detection, background subtraction, and signal intensities estimation. The quality of the spots was scored 0 or 1 (0 for bad quality, 1 for good) depending on spots radius, circularity, uniformity, and grid offset. The raw data can be found in the Gene Expression Omnibus (www.ncbi.nlm.nih.gov/geo/) under accession number GSE7686.

For the data analysis we used the MAANOVA program available on line implemented in the R statistical package. The raw signal intensities from two spots corresponding to each gene were log2 transformed and normalized within arrays using regional lowess method, which is a combination of intensity-based and special lowess methods (30). The normalized data were fitted into analysis of variance model. The analysis of variance model was a fixed effect linear model with variance terms because of array, dye, and strain effects (31). The differentially expressed genes were found by permutation test (31). Only genes that had at least one quality spot per each array were considered.

Reverse Transcriptase-PCR—RNA for RT-PCR was isolated according to van Keulen *et al.* (35) in which the usage of TRI® Reagent (Sigma) is combined with the usage of the SV total RNA isolation kit of Promega. The RNA was isolated from cells harvested during the exponential growth phase. 5 μg of RNA was mixed with 0.5 μl of 10× hexanucleotide mix (Roche Applied Science), RNase-free DNase I (Promega Corp.), and MilliQ until a final volume of 12 μl. This mixture was then heated to 70 °C for 10 min after which 4 μl of 5× first strand buffer for SuperScriptII (Invitrogen), 2 μl of 0.1 M dithiothreitol, and 1 μl of 10 mM dNTP mix (Roche Applied Science) were added. This mix was incubated for 10 min at 25 °C before adding 1 μl of RNaseOut (10 units/μl, Invitrogen) and 1 μl of SuperScriptII reverse transcriptase (200 units/μl, Invitrogen). During the incubation period at 42 °C (1 h), cDNA is made of the total RNA batch.

The PCR on cDNA template was performed with the primers listed in Table 2. The internal fragments amplified are in the range of 520–530 bp. The PCR mix contained 10–100 ng of cDNA, 1 pmol/μl of both forward and reverse primer, 2.5 mM $MgCl_2$, 5% dimethyl sulfoxide (DMSO), and 1 unit of *Taq* polymerase (Sigma). The annealing temperature was 56.5 °C, and 40 cycles were applied.

Restriction analysis on the RT-PCR products was performed following standard procedures to determine the authenticity of the products. High similarity of the *pfkA* genes causes cross-annealing of the primers producing non-gene-specific RT-PCR products. To verify identity of *pfkA1*-, *pfkA2*-, or *pfkA3*-specific products, the PCR product was cut, respectively with SacII, BglI, or HaeII (Fig. 1). As a control, a restriction was performed with any two of the aforementioned restriction enzymes. The RT-PCR products obtained were purified and concentrated prior to digestion using a GenElute PCR clean-up kit (Sigma).

Quantitative Reverse Transcriptase-PCR (qRT-PCR)—Shaking flasks of M145 and the *pfkA2* deletion strain were grown in duplicate in defined minimal medium (as described above) at 30 °C. 10 μg of RNA, extracted from cells grown for 88.5 h in defined minimal medium was treated with 10 units of DNase I (Fermentas Life Sciences) for 1 h at 37 °C. The absence of chro-

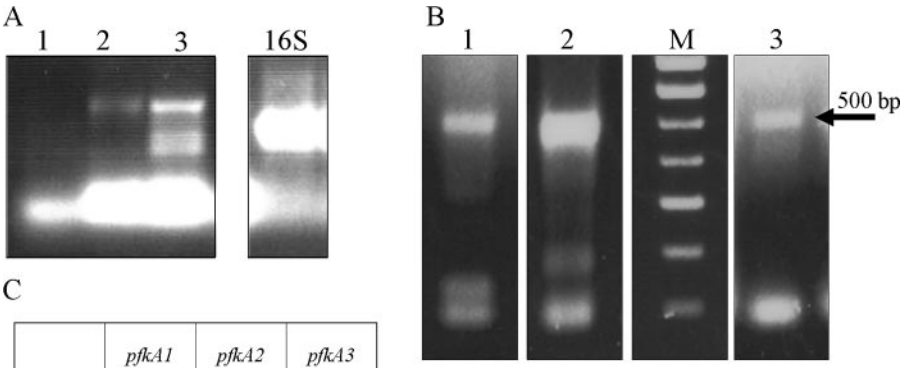

C

	pfkA1	*pfkA2*	*pfkA3*
Sac II	—	X	X
Bgl I	X	—	X
Hae II	X	X	—

FIGURE 1. *A,* RT-PCR data on *S. coelicolor* A3(2) reference strain cDNA template, created from total mRNA isolated. From *left to right,* RT-PCR products are shown that were obtained using *pfkA1*, *pfkA2*, *pfkA3*, and 16 S primers. Expected sizes of all amplified fragments range from 520 to 530 bp. *B,* restriction fragments of PCR products obtained by RT-PCR. *Lane 1* represents *pfkA2* specific PCR product amplified from the *S. coelicolor* A3(2) reference strain cDNA pool of which any false-positive signals have been removed by restriction digestion. *Lane 2* shows confirmed positive *pfkA3* signal obtained from reference strain cDNA. *Lane 3* is *pfkA3* product obtained from Δ*pfkA2* cDNA and confirmed by restriction analysis. *M* is the marker. *C,* schematic representation of the restriction digestion procedure used for confirming *pfkA* products in reverse transcriptase-PCR. Presence of recognition sites in the *pfkA* internal fragments for any of the three restriction endonucleases mentioned at the *left* of the scheme is symbolized with an *X*.

mosomal DNA contamination was checked by PCR using 16 S primers (Table 2). 2 μg of DNase I-treated mRNA was used as a template to synthesize cDNA. After incubation at 70 °C for 10 min with 1.8 μg of random hexanucleotide primers (Roche Applied Science), 5× First-Strand Buffer, dithiothreitol (10 mM), dNTPs (1 mM), and 100 units of Superscript II (Invitrogen) were added to a final volume of 30 μl. The mixture was incubated at 50 °C for 100 min followed by 15-min incubation at 75 °C.

qRT-PCR was performed in 96-micro-well plates using the ABI Prism 7500FAST system (Applied Biosystems). Each 25-μl reaction contained 12.5 μl of SYBR Green PCR Master Mix (Applied Biosystems), 10 ng of cDNA, 10 pmol of each primer, and 9.5 μl of water. The reaction parameters were as follows: 95 °C for 10 min, followed by 40 two-step amplification cycles consisting of 30 s denaturation at 95 °C and 1 min of annealing and extension at 60 °C. A final dissociation stage was run to generate a melting curve and consequently verify the specificity of the amplification products. Real time PCR was monitored and analyzed by the sequence detection system version 1.3 (Applied Biosystems), and relative expression levels were normalized to mRNA of the major vegetative sigma factor (*hrdB*). All samples were run in triplicate. The genes studied were *redD*, *redQ*, *actII-orf4*, and *actIII*. Primer sequences are shown in Table 2.

Identifying Reporter Metabolites and Significantly Co-regulated Metabolic Sub-networks—An algorithm by Patil and Nielsen (32) and an *S. coelicolor* genome-scale metabolic model (26) were used for identifying reporter metabolites and transcriptionally co-regulated metabolic sub-networks.

Metabolic Modeling—A genome-scale metabolic model of *S. coelicolor* A3(2) containing 700 unique reactions was used for metabolic modeling (26). For calculating fluxes in the wild type strain, the glucose uptake rate was set to the experimental value, and the fluxes through $NADP^+$-dependent glucose-6-phosphate 1-dehydrogenase, phosphofructokinase, isocitrate dehydrogenase, and through the reactions leading from pyruvate to acetyl-CoA were constrained to the values determined from ^{13}C metabolic flux analysis for the wild type strain. The flux distribution was obtained by linear optimization for growth using the LINDO program (Lindo Systems). To simulate the fluxes in the mutants, the flux through phosphofructokinase was set to decreasing values, and the new flux distribution was found by using the MOMA approach (33) using in-house developed software (34).

Preparation of Extracts and Enzyme Activity Assays—Cells used for activity assays were harvested after 67 h of growth in 200 ml of defined medium in a 1-liter flask equipped with a stainless steel spiral. Cells were harvested by centrifugation and resuspended in buffer containing 50 mM TES, pH 7.2, 5 mM $MgCl_2$, 5 mM 2-mercaptoethanol, 50 mM $(NH_4)_2SO_4$, and 0.1 mM phenylmethylsulfonyl fluoride (buffer A), and disrupted by sonication until >90% of the cells were lysed.

Pfk activity assays were based on the consumption of NADH in a coupled assay, according to Alves *et al.* (15). Glucose-6-phosphate dehydrogenase (G6PDH, EC 1.1.1.49) assays were based on the production of NADPH and performed according to the protocol of Lessie and Wyk (36) and modified by Butler *et al.* (3). Both the consumption of NADH and the production of NADPH were measured spectrophotometrically at 340 nm. Protein concentrations were determined using the Bio-Rad protein assay reagent and a bovine serum albumin-based standard curve.

RESULTS

Deletion of Phosphofructokinase Isoenzymes Influences Antibiotic Production—The *S. coelicolor* reference strain as well as its isogenic mutants Δ*pfkA1*, Δ*pfkA2*, and Δ*pfkA3* were grown in complex (R2YE) media in shake flasks, and the pigmented antibiotics ACT and RED were quantified over the course of several days (Fig. 2, *A* and *B*). Morphology of the *pfkA* single deletion mutants did not differ from that of the parent strains, neither in liquid media nor on solid media. When grown in R2YE liquid medium the Δ*pfkA2* mutant had a 2–6-fold increased antibiotic production compared with the reference

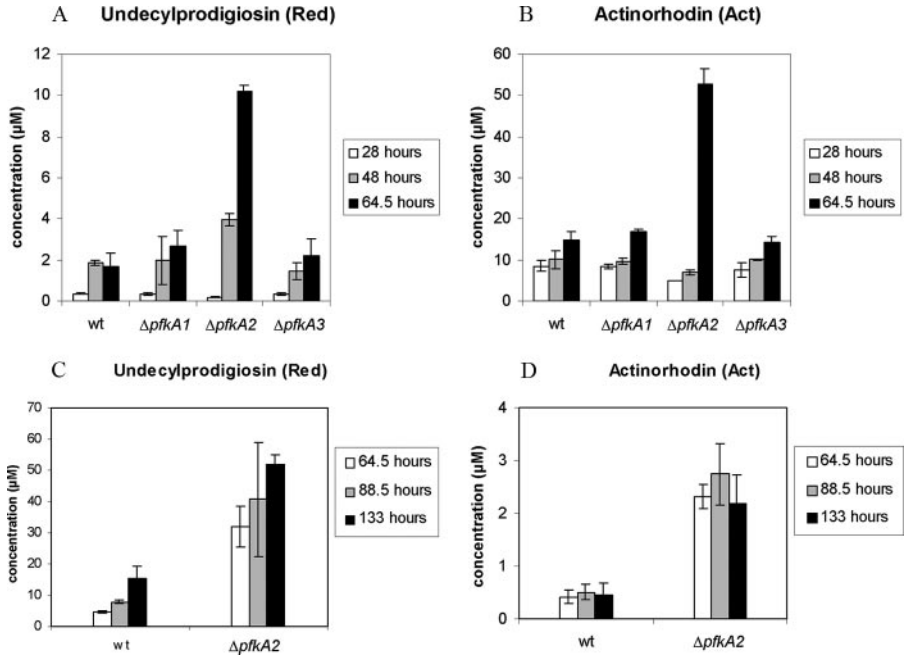

FIGURE 2. **Quantification of RED and ACT in R2YE (*A* and *B*) and defined minimal medium (*C* and *D*) grown cultures of the *S. coelicolor* A3(2) reference strain and the *pfkA* deletion strains.** Concentrations of ACT and RED produced were determined after 28, 48, and 64.5 h (R2YE) or 64.5, 88.5, and 133 h (MM) of growth in shake flasks, corresponding to exponential, early stationary, and late stationary phases. The *error bars* indicate standard deviation between biological triplicates. *wt*, wild type.

TABLE 3

Growth parameters of the *S. coelicolor* A3(2) reference and Δ*pfkA2* mutant strains as determined in controlled fermentations in defined medium

Growth parameters	M145[a]	M145 Δ*pfkA2*[b]
Maximal specific growth rate, μ_{max}, h^{-1}	0.11 ± 0.01	0.09 ± 0.02
Biomass yield on glucose, Y_{SX}, g (dry weight)/g glucose	0.39 ± 0.02	0.31 ± 0.02
Specific glucose uptake rate, R_s, mmol glucose/g (dry weight)/h	1.57 ± 0.14	1.61 ± 0.40
CO_2 yield on glucose, Y_{SC}, mmol CO_2/g (dry weight)	44 ± 7	54 ± 7
Carbon balance closure[c]	94 ± 9%	84 ± 4%

[a] Average values and standard deviations calculated from four independent cultivations.
[b] Average values and standard deviations calculated from three independent cultivations.
[c] Closusre is assuming 5% ash content in the biomass and average biomass composition $CH_{1.81}O_{0.58}N_{0.2}S_{0.004}P_{0.01}$.

strain. This was in contrast with the *pfkA1* and *pfkA3* single deletion mutants, which produced ACT and RED in quantities comparable with that of the reference strain. The ACT and RED overproduction by the *pfkA2* deletion strain was most pronounced after 64.5 h of growth when the culture entered the stationary phase. The ACT and RED overproduction phenotype in Δ*pfkA2* was also observed in defined medium (Fig. 2, *C* and *D*). Because of its antibiotic overproduction characteristics, the Δ*pfkA2* strain was selected for more detailed analysis.

Deletion of pfkA2 Influences Biomass Yield—The reference M145 strain and the Δ*pfkA2* mutant were grown in phosphate-limited defined mineral medium with glucose as the only carbon source in well controlled fermentors to estimate growth parameters (Table 3). The maximal specific growth rates were not significantly different when accounting for the standard deviation (0.09 ± 0.02 and 0.11 ± 0.01 h^{-1}); however, the mutant had a lower biomass yield on glucose (0.31 ± 0.02 against 0.39 ± 0.02 g (dry weight)/g glucose). The mutant strain was also characterized by a slightly larger specific carbon dioxide production, 54 ± 7 mmol of CO_2/g (dry weight) compared with 44 ± 7 mmol of CO_2/g (dry weight) in the reference strain (93% confidence level). HPLC analysis of the fermentation broth of the Δ*pfkA2* cultures revealed the presence of small amounts of acetate, which was not found in the reference cultivations.

The ΔpfkA2 Strain Accumulates Glucose 6-Phosphate—We speculated that limited phosphofructokinase capacity in the Δ*pfkA2* strain resulted in intracellular accumulation of the substrate for this enzyme, fructose 6-phosphate. As the isomerization between fructose-6-P and glucose-6-P is generally close to equilibrium, we expected to see elevated levels of glucose-6-P as well. Both strains were grown in triplicate shake flasks, and the samples for intracellular sugar phosphate analysis were taken 24 h after inoculation. At this point the biomass concentration was about 2 g/liter, and the cells were in the exponential growth phase. Cold methanol quenching was applied. Because previous reports on actinomycetes (37) suggest leakage caused by cold shock, we measured the sugar phosphates both in extracts of biomass and in the quenching liquid. Indeed, we found that 94–97% of the metabolites had leaked out of the cells during the quenching with cold methanol. The method was, however, still suitable for our assay, because glucose-6-P and fructose-6-P do not freely diffuse across membranes and are normally not found outside cells; all sugar phosphates in the quenching liquid should therefore be of intracellular origin.

Glucose 6-phosphate concentration was higher in the mutant (6.9 ± 0.2 μmol/g (dry weight)) than in the reference strain (5.2 ± 0.4 μmol/g (dry weight)). Fructose 6-phosphate concentration was also higher at 90% confidence level as follows: 1.9 ± 0.4 μmol/g (dry weight) for the mutant and 1.4 ± 0.4 μmol/g (dry weight) for the reference strain. The ratio between fructose-6-P and glucose-6-P concentrations was 1:3.6 in both strains.

The results were consistent with data in yeast, where deletions of one or two subunits of phosphofructokinase also resulted in accumulation of intracellular hexose monophosphates (38). Another reported effect in yeast is the accumulation of storage carbohydrates glycogen and trehalose (39), carbohydrates that are also produced by *S. coelicolor* (40–42). We could not detect glycogen in the late stationary phase of the liquid cultures of either the reference or the mutant strain (data not shown). The total carbohydrate content in stationary phase cultures was not significantly different between the two strains

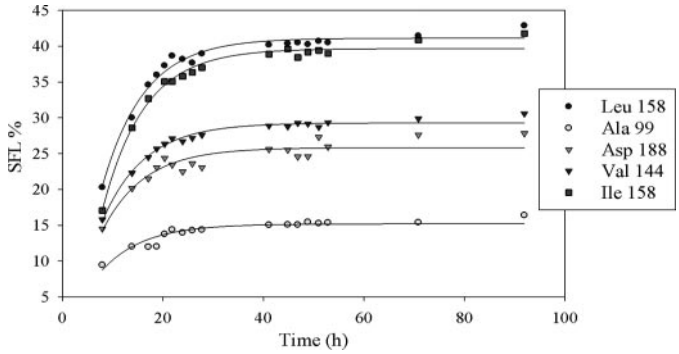

FIGURE 3. **SFL values of leucine, alanine, aspartate, valine, and isoleucine fragments as a function of time in the *S. coelicolor* A3(2) reference strain (the number next to the amino acid abbreviation is the *m/z* value).** The labeling of the amino acids fragments follows first order kinetics. Fermentations with the *S. coelicolor* A3(2) reference strain and the Δ*pfkA2* strain were performed with 30% [1-^{13}C]glucose as carbon source. Samples for biomass measurements were taken during cultivations, and the labeling of proteinogenic amino acids was measured using gas chromatography coupled to mass spectrometry.

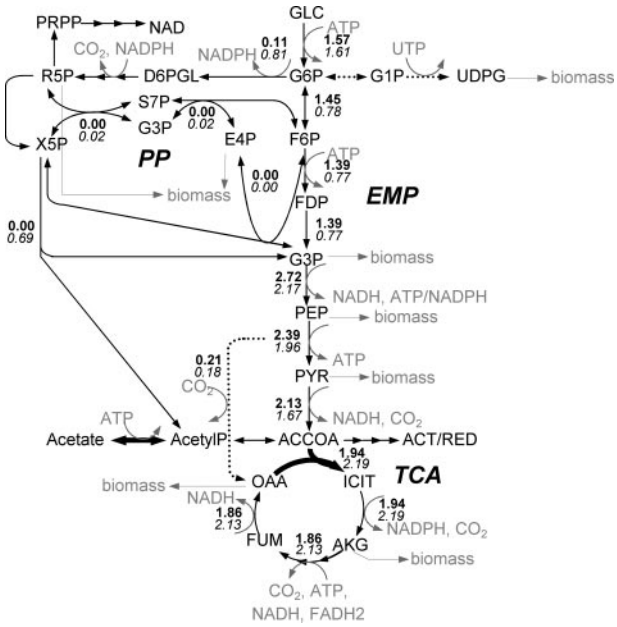

FIGURE 4. **Changes in intracellular fluxes in the Δ*pfkA2* mutant strain compared with the *S. coelicolor* A3(2) reference strain.** The standard deviation of flux estimation did not exceed 5%. All fluxes are expressed in mmol/g(dry weight)/h. The enzymes that are part of significantly co-regulated metabolic sub-network are *highlighted*. The whole sub-network can be found in supplemental Fig. S6. Genes up-regulated in the mutant are shown with *thick lines* and down-regulated with *dotted lines*. The reaction catalyzed by phosphoketolase and leading from fructose 6-phosphate into erythrose 4-phosphate and acetyl phosphate is not shown to avoid crowdedness of the figure. The flux through it was 0.02 for the reference strain and 0.00 for the mutant strain. The abbreviations used are as follows: *GLC*, glucose; *G6P*, glucose 6-phosphate; *G1P*, glucose 1-phosphate; *UDPG*, UDP-glucose; *F6P*, fructose 6-phosphate; *FDP*, fructose 1,6-bisphosphate; *D6PGL*, glucono-1,5-lacton-6-phosphate; *R5P*, ribose 5-phosphate; *PRPP*, 5-phosphoribosyl diphosphate; *X5P*, xylulose 5-phosphate; *S7P*, seduheptulose 7-phosphate; *E4P*, erythrose 4-phosphate; *G3P*, glyceraldehyde 3-phosphate; *PEP*, phosphoenolpyruvate; *PYR*, pyruvate; *ACCOA*, acetyl-CoA; *ACT*, actinorhodin; *RED*, undecylprodigiosin; *ICIT*, isocitrate; *AKG*, a-ketoglutarate; *FUM*, fumarate; *OAA*, oxaloacetate; *AcetylP*, acetyl phosphate.

as follows: 13 ± 3% of dry weight for the reference strain and 15 ± 2% for the mutant.

The Δpfk A2 Strain Has an Increased Flux through the Pentose Phosphate Pathway—Fermentations with the M145 and Δ*pfkA2* strains were performed with 30% 1-^{13}C-labeled glucose as the carbon source. Samples for biomass measurements were taken during cultivations, and the labeling of proteinogenic amino acids was measured using gas chromatography coupled to mass spectrometry. Labeling of most of the amino acid fragments followed first order kinetics according to the equation: $SFL = SFL_0 + (SFL_\infty - SFL_0) \times (1 - e^{-\mu t})$ (Fig. 3 and supplemental Fig. S3), where SFL_0 stands for initial labeling of the fragment, and SFL_∞ describes the steady state labeling after all the unlabeled proteins from the inoculum cells had been substituted by proteins synthesized from labeled glucose. Labeling of most of the fragments had reached steady state by the end of the exponential phase. There were no clear changes in the labeling of amino acids after the end of the exponential growth phase, implying that flux distribution in the stationary phase was similar to that of the exponential phase. SFL_∞ values together with growth parameters were used to calculate the intracellular fluxes (Fig. 4 and supplemental Fig. S3).

The label distribution in the amino acids reflects the pathways by which amino acid precursors were synthesized. Labeling of alanine and valine gives information about the glycolytic pathway, which leads to the formation of pyruvate. With an active Entner-Doudoroff (ED) pathway present, half of the pyruvate made from [1-^{13}C]glucose would be labeled at the carboxylic group (first position). The percentage of labeling of that atom was around 3% (deduced from fragments Ala-158, Ala-116, and Ala-99) and close to the natural labeling of 1.1% (supplemental Fig. S3). Also the first and second atoms of phosphoenolpyruvate (fragment Phe-143) were slightly labeled. Therefore, we conclude that the label in pyruvate was not supplied by an ED pathway but was the result of scrambling in the PPP and/or activity of phosphoenolpyruvate carboxykinase or malic enzyme, feeding label from the tricarboxylic acid cycle. In the oxidative branch of the pentose phosphate pathway, the first carbon atom of glucose does not get incorporated in pyruvate but is oxidized, producing carbon dioxide. In case of glucose labeled at C-1, the label will be lost, and all pyruvate resulting from this pathway will be nonlabeled. The higher the flux through the PPP, the fewer ^{13}C heavy isotopes will get incorporated into pyruvate and into tricarboxylic acid cycle intermediates. In the reference *S. coelicolor* strain the labeling of the second and third carbon atoms of pyruvate at the end of cultivation (Ala-99 and Ala-116) reached 16.4–16.6%, which is close to the theoretical maximum if all pyruvate is generated through the EMP, meaning that the pentose phosphate flux was very low. For the mutant strain the corresponding labeling value was 14.2–14.5%, indicating higher PPP flux. The labeling of pyruvate and tricarboxylic acid cycle intermediates (oxaloacetate and α-ketoglutarate) was lower in the Δ*pfkA2* strain, which also indicates a higher flux through the PPP in the mutant.

The labeling of acetyl-CoA second carbon atom as calculated from fragment Leu-158 was lower than the labeling of the third carbon atom of pyruvate. This indicates that not all acetyl-CoA is coming directly from pyruvate, but some can be supplied through other pathways that have lower labeling. It could be the phosphoketolase pathway. Phosphoketolase Xpk (EC 4.1.2.9) catalyzes the cleavage of xylulose 5-phosphate into glyceraldehyde 3-phosphate and acetyl phosphate as well as cleavage of

fructose 6-phosphate into erythrose 4-phosphate and acetyl phosphate. The activity of this enzyme has been measured mostly during growth on pentoses in *Bifidobacteria* (43, 44), several *Lactobacillus* species (45, 46), *Saccharomyces cerevisiae* (47), and others. BLASTing with Xpk protein sequence of *Bifidobacterium adolescentis* against the whole genome of *S. coelicolor* A3(2) gave a hit to a probable phosphoketolase SCO0617 with 49% identity. In the initial genome annotation this protein was noted as hypothetical (11).

For flux calculations we included the EMP and PPP glycolytic pathways, phosphoketolase reactions, and the tricarboxylic acid cycle. The anaplerotic glyoxylate shunt was considered to be inactive on glucose (48), so only pyruvate and phosphoenolpyruvate carboxylases were included. It is not possible to discriminate between these two reactions with high confidence when the first carbon of pyruvate is not labeled, hence the summed anaplerotic flux is shown in Fig. 4. We did not account for acetate secretion because only small amounts, below 0.1 g/liter, were detected in the late broth samples of the mutant strain.

For *S. coelicolor* M145, 7% of the imported glucose went into the oxidative branch of the pentose phosphate pathway (supplemental Fig. S4). This pathway is involved in generation of precursors for nucleotide biosynthesis (ribose 5-phosphate) and aromatic amino acids (erythrose 4-phosphate). Because there was no back-flux from the PPP into glycolysis, the main role of the PPP was generation of biomass precursors.

In the Δ*pfkA2* mutant strain as much as 50% of the imported glucose was shunted toward the pentose phosphate pathway. As the amount of precursors generated in this case exceeded the demand, most of the carbon entering the PPP was further shuffled through phosphoketolase into glyceraldehyde 3-phosphate and acetyl phosphate. The oxidation of glucose 6-phosphate into ribulose 5-phosphate usually leads to production of two NADPH molecules. In *S. coelicolor* the cofactor specificity of two glucose-6-phosphate 1-dehydrogenases (*zwf1* and *2*, SCO6661 and SCO1937 respectively) and of 6-phosphogluconate dehydrogenase (*zwf3*, SCO0975) has been determined (5). Both enzymes are $NADP^+$-dependent, which means that there was an increased NADPH production in the mutant strain. By the action of phosphate acetyltransferase acetyl phosphate can be converted into acetyl-CoA, which further enters tricarboxylic acid cycle, fatty acid metabolism, secondary metabolism, etc. Acetyl phosphate can also be hydrolyzed by acylphosphatase into acetate. The flux through the tricarboxylic acid cycle and through the anaplerotic pathways did not differ much between the reference and the mutant strains.

The Δpfk A2 Strain Produces More NADPH—To test whether the increased flux through the PPP in the mutant led to NADPH overproduction, we examined the diamide sensitivity of the strains. The test was previously used for a study of *zwf1/zwf2* negative *S. lividans* strains (3). Diamide oxidizes sulfide groups in proteins and thiols causing formation of toxic disulfide bridges. This oxidative stress is neutralized by thioredoxin reductase (28), which requires NADPH as electron donor. The more NADPH the cells can generate, the higher the supply for thioredoxin reductase, the more resistant the strain should be to diamide. The test showed a significantly reduced sensitivity of strain Δ*pfkA2* to diamide (at $p > 95\%$), whereas strains Δ*pfkA* or Δ*pfkA3* were not significantly different to wild type (Table 4). The halo surface surrounding the 0.5 M diamide impregnated disk, measured 890.4 ± 30.4 mm^2 for the wild type *versus* 812.7 ± 14.6 mm^2 for strain Δ*pfkA2*.

TABLE 4

Sensitivity of *S. coelicolor* A3(2) M145 strain and *pfkA* deletion mutants to 0.5 M diamide

The table shows the diameter and area of the halo formed around a disk impregnated with diamide.

Strain	Diameter	Surface
	mm	mm^2
M145	33.7 ± 0.6	890.4 ± 30.4
Δ*pfkA1*	33.3 ± 0.3	872.7 ± 15.1
Δ*pfkA2*	32.2 ± 0.3	812.7 ± 14.6
Δ*pfkA3*	33.0 ± 0.5	855.4 ± 25.9

Reverse Transcriptase-PCR—High similarity of the three *pfkA* genes prevents discrimination between their transcripts on microarrays. This was also evident from our array studies, showing no significant change in *pfkA2* expression for the *pfkA2* deletion strain, indicating cross-hybridization by *pfkA1* and/or *pfkA3* mRNA (supplemental Fig. S5). A combination of RT-PCR with restriction digestion, however, does allow detection and discrimination of mRNA of a single *pfkA*. RT-PCR revealed the presence of *pfkA2* and *pfkA3* mRNA in M145 grown on minimal medium (Fig. 1). The cells were harvested in the exponential growth phase. This finding is in accordance to that of Hesketh *et al.* (49) who detected PfkA2 and PfkA3 protein spots on two-dimensional gels of *S. coelicolor* grown under comparable conditions (SMM phosphate-limited minimal medium). As anticipated, only the presence of *pfkA3* mRNA was detected in mRNA isolated from the *pfkA2* deletion strain harvested at the same time point. The authenticity of the RT-PCR products was confirmed by restriction analysis, to exclude products formed because of cross-annealing of the primers.

Pfk and G6PDH Activity Assays—To study differences in G6PDH and Pfk activities, enzyme assays were performed on *S. coelicolor* crude extracts. G6PDH assays did not reveal significant differences in activity between *pfkA2* deletion mutants and their parent strain (166 ± 37 μmol/min/mg protein). The specific activity of ATP-dependent Pfk in cell extracts of M145 grown on R2YE was 0.072 ± 0.027 μmol/min/mg, which compares to ATP-dependent Pfk-specific activities of, respectively, 0.073 ± 0.013 μmol/min/mg measured for M145 grown on YEME (15). Pfk activities, whether ATP-, PP_i-, ADP-, or polyphosphate-dependent, could not be determined in cell extracts of strain Δ*pfkA2*, whereas wild type-like ATP-dependent Pfk activities could readily be measured in cell extracts of mutant strains Δ*pfkA1* and Δ*pfkA3*, which still contain a copy of the ATP-dependent Pfk gene *pfkA2*.

Deletion of pfkA2 Causes Transcriptional Changes in Regulatory and Membrane Proteins as Well as in Fatty Acid Metabolism—The effect of the *pfkA2* deletion on gene expression was studied by comparison of RNA of the *S. coelicolor* A3(2) reference and mutant strains using spotted DNA microarrays. RNA was isolated from cultures in the mid exponential growth phase.

The 588 genes that had a *p* value below 0.05 in permutation test, and for which there was at least one quality spot per each

TABLE 5

Genes that are significantly ($p < 0.05$) up- or down-regulated (boldface type) in the Δ*pfkA2* mutant in comparison with the *S. coelicolor* A3(2) reference strain

The genes are sorted by functional categories, and for each category the *p* value from hypergeometric distribution is shown.

Functional category	Differentially expressed	Total number in genome	*p* value[a]
Transcriptional regulators and other regulatory proteins	**48**	**460**	**0.01**
Degradation of fatty acids	**9**	**58**	**0.02**
Gram-positive membrane	**72**	**826**	**0.09**
Ribosomal proteins, synthesis, modification	6	62	0.20
Secondary metabolism	24	276	0.21
Gram positive peptidoglycan, teichoic acid	4	40	0.23
Cell division	3	20	0.27
Sensor kinase	7	86	0.33
Degradation of proteins, peptides, glycoproteins	10	126	0.36
Degradation of carbon compounds	7	90	0.38
Cation transport	3	39	0.39
Transposon/insertion element-related functions	4	58	0.46
Non-classified	42	559	0.49
Response regulators and sigma factors	12	167	0.51
Gram positive exported lipoprotein	32	438	0.55
Fatty acid and phosphatidic acid biosynthesis	3	53	0.60
Transport/binding proteins	36	518	0.69
Macromolecule synthesis, modification	16	247	0.70
Degradation of polysaccharides	5	92	0.71
Electron transport	3	70	0.79
Detoxification	2	88	0.97
Others	62	1017	
Unknown function	178	2336	
Total	588	7726	

[a] The *p* value shows has the detected or higher number of genes from a particular functional category among the differentially expressed genes. Data were calculated according to Equation 2. Small *p* values indicate functional categories that were most affected by the mutation.

array, were considered to be differentially expressed (supplemental Fig. S5). The genes were sorted into functional categories according to a protein classification scheme proposed by the Sanger Institute. Functional categories that were most influenced by the genetic change were determined by hypergeometric distribution and included fatty acid metabolism, regulatory genes, and membrane proteins (Table 5; *p* values having the detected or high number of genes from a particular category among the differentially expressed genes was calculated according to Equation 2,

$$p = 1 - \sum_{i=0}^{x} \frac{\binom{M}{i}\binom{N-M}{K-i}}{\binom{N}{K}} \qquad \text{(Eq. 2)}$$

where N indicates the total genes analyzed on the chip; K indicates differentially expressed genes; M indicates the genes from a particular functional category present on the chip, and x is the number of differentially expressed genes that belong to that functional category.)

Of the ~460 transcriptional regulators and regulatory proteins that were annotated in the *S. coelicolor* genome, 46 changed their expression significantly in the Δ*pfkA2* mutant. As the exact role and binding sites are not known for most of the transcriptional regulators, it is difficult to say what influence their changed expression has on the cells. One of them is, however, a better studied A-factor receptor homologue, CprB (SCO6071) (50). In contrast to another A-factor receptor homologue, CprA (SCO6312), which acts as a positive regulator of secondary metabolism and sporulation, CprB seems to have an opposite role (51). Deletion of CprB caused increased actinorhodin production and earlier sporulation (51). This gene was down-regulated in the Δ*pfkA2* mutant. Another gene with a better studied function was the *recX* gene (SCO5770), which was expressed slightly higher in the mutant. *recX* is positioned downstream of the *recA*-encoded recombinase and is most probably involved in its down-regulation (52–55). *recX* transcripts were previously detected in *S. lividans* only under DNA-damaging conditions (56).

Fatty acids are building blocks of phospholipids and glycolipids used in the cytoplasmic membrane, as well as of triacylglycerols, which serve as energy storage molecules (57–59). Triacylglycerols were found in the post-exponential phase biomass of several *Streptomyces* species and were hypothesized to serve as a C-2 source for polyketide formation (57). Biosynthesis of fatty acids can also serve as a sink for NADPH, which is used during chain elongation. Subsequent degradation of fatty acids would provide ATP and NADH/$FADH_2$, the latter also coupled to ATP production through the electron transport chain. In our data set we saw significant overexpression of acyl-CoA dehydrogenases (SCO3051, SCO4681, and SCO1701) as well as lipases/esterases (SCO4746 and SCO3644).

Interestingly, the phosphofructokinase genes display a trend of increased expression. Because of the high sequence similarity between the isoenzymes, it is not possible to distinguish the species on the array. However, because *pfkA2* has been completely deleted from the mutant, the mRNA must be of *pfkA1* and/or *pfkA3* origin, which in a reaction to the loss of *pfkA2* would increase in expression. Because mRNA of *pfkA1* could not be detected with RT-PCR, the mRNA must be the result of *pfkA3* transcription.

Secondary Metabolite Gene Cluster Expression Quantified by qRT-PCR—mRNA isolated from M145 and *pfkA2* deletion strain was used for quantifying expression levels of undecylprodigiosin (*redD*, *redQ*) and actinorhodin (*actII-orf4*, *actIII*) metabolism associated genes. The RNA was isolated from cells harvested at the mid-exponential growth phase at a point in time where the medium was already pigmented. qRT-PCR revealed a 2-fold increase in *actII-orf4* ($p = 0.035$) and *actIII* ($p = 0.004$) expression in the *pfkA2* negative strain when compared with the parent strain. In contrast, differential expression of *redD* (no PCR product) and *redQ* ($p = 0.214$) was not observed.

Metabolic Sub-networks with Changed Gene Expression—Of the 588 genes with altered expression, only a minor proportion can be directly linked to the primary metabolism or to the antibiotic production. Studying metabolic sub-networks might in this case prove to be a useful tool for interpreting the effect of the *pfkA2* deletion on gene expression. Metabolic genes are interconnected through common metabolites. To avoid potentially harmful accumulation of metabolites, the activities of the enzymes that produce and consume those metabolites have to be coordinated. In bacteria, genes that belong to a linear meta-

TABLE 6

Top 20 reporter metabolites around which the most significant changes in expression occurred in the Δ*pfkA2* mutant strain

The top 20 reporter metabolites around which the most significant changes in expression occurred in the Δ*pfkA2* mutant strain were compared with the *S. coelicolor* A3(2) reference strain identified using an algorithm by Patil *et al.* (32) and an *S. coelicolor* genome-scale metabolic model (26), to define connections between metabolites and the enzymes that have these metabolites as substrates or products. Only metabolites that have more than one neighbor have been considered.

Metabolite	Processes	No. of neighbors	*p* value
D-Glucose 1-phosphate	Storage carbohydrates	2	0.00
D-Galactose 1-phosphate	Storage carbohydrates	2	0.07
UTP	Pyrimidines/storage carbohydrates/Peptidoglycan	5	0.02
N^6-(1,2-Dicarboxyethyl)-AMP	ATP biosynthesis	2	0.05
NADH	Reducing cofactor	49	0.04
D-Ribose 5-phosphate	Pentose phosphate pathway	9	0.08
2,3,4,5-Tetrahydrodipicolinate	Amino acids metabolism	2	0.04
L-Lysine	Amino acids metabolism	3	0.07
3-Phosphonooxypyruvate	Amino acids metabolism	2	0.00
L-Homoserine	Amino acids metabolism	2	0.00
L-Histidine	Amino acids metabolism	3	0.02
L-Aspartate	Amino acids metabolism	12	0.03
L-Aspartate 4-semialdehyde	Amino acids metabolism	4	0.03
2-Dehydro-3-deoxy-D-arabinoheptonate 7-phosphate	Amino acids metabolism	2	0.07
Acetaldehyde	Pyruvate metabolism	7	0.01
Ethanol	Pyruvate metabolism	3	0.02
Propionyl phosphate	Propanoate metabolism	2	0.02
Propanoate	Propanoate metabolism	4	0.04
Methylmalonate semialdehyde	Propanoate metabolism	7	0.08
Oxaloacetate	Tricarboxylic acid cycle/anapleurotic reactions	11	0.03

bolic pathway often are positioned in one operon to ensure their coordinated expression. When an enzyme is deleted or overexpressed, the cells will seek to maintain metabolic *status quo* by changing the activities of connected enzymes, either at the transcriptional level or at the protein level.

To further analyze the transcriptional response to the deletion of *pfkA2,* we identified metabolites around which the most significant changes in expression occurred (Table 6). For this purpose we used a genome-scale metabolic model to define connections between metabolites and the enzymes that have these metabolites as substrates or products (32). The significance of the gene expression test, expressed as *p* values from the permutation test, were used for each metabolic gene included in the model.

Among the high scoring reporter metabolites were glucose 1-phosphate and galactose 1-phosphate, precursors for storage carbohydrates, which indicate transcriptional changes in this route. Increased accumulation of storage carbohydrates was observed in yeast lacking phosphofructokinase (39), although we could not detect that in *S. coelicolor* (see above). Another top scoring reporter metabolite is the reducing co-factor NADH. This cofactor participates in 62 reactions in the model, and the low *p* value indicates that transcriptional changes occurred in many of the neighboring enzymes. Some other reporter metabolites were from amino acid biosynthesis and degradation pathways. Amino acid biosynthesis leads to oxidation of NADPH into $NADP^+$ and can be connected to the altered level of this co-factor. There were changes in pyruvate and propanoate metabolism, which supply precursors for polyketide compounds. The presence of oxaloacetate among reporter metabolites can indicate both transcriptional changes in the tricarboxylic acid cycle and anaplerotic reactions. Remarkably, significant transcriptional changes occurred around ribose 5-phosphate, a key metabolite of the pentose phosphate pathway and nucleotide precursor.

The enzymes can be represented in the form of a network, where the enzymes act as nodes and the shared substrates make the edges. In this metabolic network significantly regulated sub-networks can be found (32). Genes linked to the most significant sub-networks are highlighted in Fig. 4. The sub-network included citrate synthase *citA* (SCO2736), which is homologous to the principal isoenzyme in the *S. coelicolor* wild type strain MT1110 (7). Deletion of this enzyme causes this strain to become auxotrophic for glutamate and leads to severe acidification of medium with acetate, pyruvate, and other organic acids (7). CitA was up-regulated in our mutant strain. Another up-regulated enzyme, which is also part of the most significantly regulated sub-network, was acetate kinase (SCO5424). The analysis indicates some transcriptional changes around the acetyl-CoA node, which is also consistent with the low acetate secretion by the mutant strain. The sub-network also included RNA synthesis, which is primarily catalyzed by α- (SCO4729), β- (SCO4654), and ω- (SCO1478) RNA polymerase subunits. In the mutant, α-, β- and ω-chains of RNA polymerase were down-regulated, the former two at a 95% and the latter at an 85% significance level.

Metabolic Modeling—For the purpose of metabolic engineering, it is a great advantage to be able to predict which genetic changes will lead to a desired phenotype. Genome-scale metabolic models have been used recently for making such predictions (60, 61). We were interested to see what phenotype the existing *S. coelicolor* genome-scale metabolic model would suggest for decreased phosphofructokinase activity.

The model contains 700 unique reactions, many of which are reversible, hence the degree of freedom is very high, and the model can therefore not be used to obtain precise estimates of the intracellular fluxes without the addition of some constraints. By including a few constraints from the ^{13}C metabolic flux analysis calculations (restrictions of the PPP flux, the tricarboxylic acid flux, and the EMP flux), the model could predict the specific growth rate to be 0.1 h^{-1} when the specific glucose uptake rate was set at 1.57 mmol/g (dry weight)/h. This is very close to the actual value (Table 3), and hence we assumed that the predicted fluxes were a good reflection of the actual fluxes in the cell.

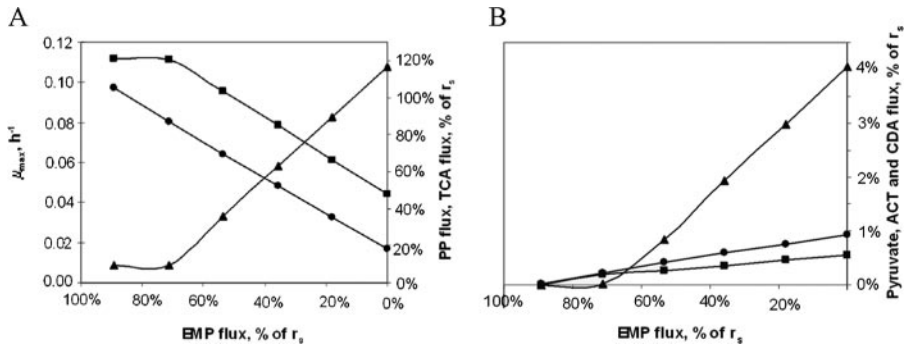

FIGURE 5. ***S. coelicolor* genome-scale metabolic model predicted effects of decreased flux through phosphofructokinase in the Δ*pfkA2* mutant strain on the following: growth rate (●), pentose phosphate flux (▲), and tricarboxylic acid cycle flux (■) (*A*), and on pyruvate excretion (▲), actinorhodin (■) flux and calcium-dependent antibiotic flux (●) (*B*).**

Using the obtained wild type flux distribution, we predicted how the fluxes would change with a decrease in the EMP flux. We assumed that the cells will undergo as few flux changes as possible to adjust to the new conditions; hence we chose a minimization of flux adjustment (MOMA) approach for the simulations (33).

First, the model predicted excretion of compounds, which were not detected experimentally and were not reported earlier to be produced during *S. coelicolor* fermentations, *e.g.* acetate, acetaldehyde, ethanol, formate, and proline. When the secretion of these compounds was constrained to zero, the model predicted pyruvate-, actinorhodin-, and calcium-dependent antibiotic as fermentation products (Fig. 5). The decrease of flux through phosphofructokinase correlated with decreased specific growth rate and an increased flux through the PPP, and the latter was also observed experimentally.

DISCUSSION

In this study the effects of the deletion of *pfkA2* (SCO5426) on metabolic fluxes in *S. coelicolor* were studied. The most obvious physiological effect of this deletion was an increase in production of the pigmented antibiotics ACT and RED on both minimal and rich media without a significant decrease in specific growth rate.

A direct link between primary and secondary metabolism in streptomycetes has been demonstrated before. In *S. lividans*, a close relative of *S. coelicolor*, deletion of 1 of 2 *zwf* genes led to an increase in ACT and RED production with an unaltered specific growth rate (3). The *zwf* gene products, glucose-6-phosphate 1-dehydrogenase, catalyze the first reaction of the pentose phosphate pathway. The authors explained their results by increased carbon availability for antibiotic biosynthesis pathways when less carbon was oxidized to carbon dioxide in the pentose phosphate pathway. Another group performed metabolic flux analysis on the physiological data from *S. lividans* chemostats and also hypothesized that decreased flux through the PPP would result in increased antibiotic production (62). This hypothesis was tested in *S. coelicolor* by Ryu *et al.* (5), who partially blocked the flow into the PPP by deleting *zwf* and increased actinorhodin precursor availability by overexpressing acetyl-CoA carboxylase. Deleting the main Zwf activity (*zwf2*), however, caused enhanced mycelial growth and a decreased specific ACT production rate. These results were in contradiction to the ones obtained for *S. lividans* (3). In both *S. lividans* and *S. coelicolor* the deletion of a *zwf* gene did lead to a decrease in G6PDH-specific activity. However, it should be noted that *in vivo* fluxes do not obligatorily correlate with the *in vitro* measured enzymatic activity; therefore, it is not clear how the flux through PPP was influenced in these studies.

These varying observations can be explained in terms of metabolite overflow. Accumulation of primary metabolites can be potentially harmful to an organism. Excess metabolites can be disposed of through the production of waste products, possibly the original function of the relatively ancient secondary metabolic pathways. The major evolutionary driving force for secondary metabolite synthesis, however, may subsequently have become that of fitness increase because of their bioactivity (63). Nevertheless, the overflow concept still gives a foundation for speculation on the link between primary and secondary metabolism. In light of this hypothesis, any gross metabolic imbalance that cannot be dealt with by tweaking primary metabolic pathways would stimulate production of secondary metabolites.

This study did not focus on decreasing the C-flow through the PPP but instead on decreasing the flux through glycolysis. Glycolysis is not completely blocked in the Δ*pfkA2* mutant, as demonstrated by the metabolic flux analyses, despite our inability to find remaining Pfk activity in Δ*pfkA2* cell extracts. The remaining Pfk activity is most likely provided by PfkA3, of which mRNA could be traced using reverse transcriptase-PCR. Failure to detect this PfkA3 activity may be due to enzyme instability during extract preparation or the requirement for specific assay conditions that we have not been able to identify. The reduction in Pfk activity in the Δ*pfkA2* mutant strain led to an accumulation of fructose-6-P and glucose-6-P. This result is consistent with data from yeast studies, where deletions of one or two subunits of phosphofructokinase also resulted in accumulation of intracellular hexose monophosphates (38). Our studies show that accumulation of glucose-6-P in *S. coelicolor* A3(2) resulted in an increased flow of carbon through the PPP, which is consistent with the increased CO_2 production by the Δ*pfkA2* mutant strain. Also a flux through xylulose-5-phosphate phosphoketolase was predicted in the Δ*pfkA2* mutant but not in the reference strain. This enzyme is usually active during growth on pentoses that provide in xylulose 5-phosphate that the cells metabolize. Apparently, a similar effect was achieved by increasing the glucose conversion through the pentose phosphate pathway. Although the labeling pattern suggests the presence of phosphoketolase activity, additional enzymatic assays should be performed for confirmation.

It is interesting to note that overexpression of PPP enzymes would not necessarily lead to increased PPP flux. The higher affinity of phosphofructokinase to fructose 6-phosphate may

cause it to be the flux controlling for the PPP flow. The final result of overexpressing PPP-related enzymes might therefore only cause a minor increase in the PPP flux. Our study indicates that because of the tight regulation in central carbon metabolism, it may be better to constrain fluxes in the metabolic network through deletion of specific flux controlling genes rather than by overexpression of genes.

We suggest that the stimulating effect of increased PPP flux on antibiotic production is at least partly because of an increase in supply of NADPH as demonstrated by increased resistance to diamide. The strains with deletions of *pfkA* or *pfkA3* genes, which did not show increased antibiotic production, were not more resistant to diamide than the reference strain. NADPH is the reducing agent used in the process of making secondary metabolites, and the PPP is one of the most important NADPH-producing pathways. A role for NADPH in enhancement of antibiotic production has also been suggested before (1). Another effect could be increased production of acetyl-CoA, which serves as the basic precursor for polyketides, because of high flux through the phosphoketolase pathway.

Transcriptional data showed changes in the expression of metabolic genes. The total number of genes that were found significantly and differentially expressed was relatively low, less than 10% of the genome. This could be expected considering that the mutation did not have a drastic effect on cellular physiology and morphological development. Interpretation of gene expression data is even further complicated by the inferior annotation of *S. coelicolor* genes as compared with more studied model organisms like *E. coli* or the yeast *S. cerevisiae*. Integrated data analysis methods have proven useful for interpretation of -omic data. For studying transcriptional changes in metabolic genes, particularly supplementing the expression data, analysis with the knowledge of the metabolic network offers advantages (32). We identified transcriptional changes in carbohydrate storage metabolism, as well as in enzymes connected to the reducing co-factor NADH, the nucleotide metabolism intermediate ribose 5-phosphate, PPP, and tricarboxylic acid cycle intermediates oxaloacetate and acetyl-CoA. These findings confirm adaptation to changes that have occurred in the central carbon metabolism.

Gene expression analysis also revealed numerous changes in the expression of regulatory proteins in the mutant, indicating that increase of antibiotic production also might be influenced by regulatory events. For instance, the indirect negative regulator of actinorhodin biosynthesis CprB was down-regulated in the mutant in the exponential growth phase. For genes directly involved in actinorhodin and undecylprodigiosin production, the microarray data were inconclusive. Additional qRT-PCR data revealed that *actII-orf4*, encoding for the actinorhodin cluster activator protein, and *actIII* (ketoacyl reductase) were over two times higher expressed in the *pfkA2* deletion strain when compared with M145 grown under the same conditions. This finding shows that overproduction of at least actinorhodin is also because of overexpression of its regulatory and synthetic genes. All the above mentioned expression analyses were performed using mRNA from mid-exponential growth phase harvested cells.

Experimentally observed effects of decreased phosphofructokinase activity were predicted using a genome-scale metabolic model. This implies that this model can be used for design of strains with further improved antibiotic production.

Acknowledgments—We thank Mervyn Bibb (John Innes Centre, UK) and Matthias Redenbach (Technical University Kaiserslautern, Germany) for providing us with S. coelicolor M145; Michael Jewett (Technical University of Denmark, Denmark) for advice and help with intracellular metabolites extraction; Hans Peter Smits (Fluxome Science, Denmark) for advice and help with analysis of sugar phosphates; Emma Laing and Vassilis Mersinias for helpful discussions on microarray analysis; Giles Velarde for assistance with uploading the microarray data to the public data base, and Davide D'Alia and Martha Merrow (Rijksuniversiteit Groningen) for help with the qRT-PCR.

REFERENCES

1. Gunnarsson, N., Eliasson, A., and Nielsen, J. (2004) *Adv. Biochem. Eng. Biotechnol.* **88,** 137–178
2. Bibb, M. J. (2005) *Curr. Opin. Microbiol.* **8,** 208–215
3. Butler, M. J., Bruheim, P., Jovetic, S., Marinelli, F., Postma, P. W., and Bibb, M. J. (2002) *Appl. Environ. Microbiol.* **68,** 4731–4739
4. Li, R., and Townsend, C. A. (2006) *Metab. Eng.* **8,** 240–252
5. Ryu, Y. G., Butler, M. J., Chater, K. F., and Lee, K. J. (2006) *Appl. Environ. Microbiol.* **72,** 7132–7139
6. Viollier, P. H., Nguyen, K. T., Minas, W., Folcher, M., Dale, G. E., and Thompson, C. J. (2001) *J. Bacteriol.* **183,** 3193–3203
7. Viollier, P. H., Minas, W., Dale, G. E., Folcher, M., and Thompson, C. J. (2001) *J. Bacteriol.* **183,** 3184–3192
8. Chouayekh, H., and Virolle, M. J. (2002) *Mol. Microbiol.* **43,** 919–930
9. Ghorbel, S., Smirnov, A., Chouayekh, H., Sperandio, B., Esnault, C., Kormanec, J., and Virolle, M. J. (2006) *J. Bacteriol.* **188,** 6269–6276
10. Ghorbel, S., Kormanec, J., Artus, A., and Virolle, M. J. (2006) *J. Bacteriol.* **188,** 677–686
11. Bentley, S. D., Chater, K. F., Cerdeno-Tarraga, A. M., Challis, G. L., Thomson, N. R., James, K. D., Harris, D. E., Quail, M. A., Kieser, H., Harper, D., Bateman, A., Brown, S., Chandra, G., Chen, C. W., Collins, M., Cronin, A., Fraser, A., and Goble, A. (2002) *Nature* **417,** 141–147
12. Cole, S. T., and Barrell, B. G. (1998) *Novartis Found. Symp.* **217,** 160–177
13. Camus, J. C., Pryor, M. J., Medigue, C., and Cole, S. T. (2002) *Microbiology* **148,** 2967–2973
14. Kalinowski, J., Bathe, B., Bartels, D., Bischoff, N., Bott, M., Burkovski, A., Dusch, N., Eggeling, L., Eikmanns, B. J., Gaigalat, L., Goesmann, A., Hartmann, M., Huthmacher, K., Kramer, R., Linke, B., McHardy, A. C., Meyer, F., Mockel, B., Pfefferle, W., Puhler, A., Rey, D. A., Ruckert, C., Rupp, O., Sahm, H., Wendisch, V. F., Wiegrabe, I., and Tauch, A. (2003) *J. Biotechnol.* **104,** 5–25
15. Alves, A. M., Euverink, G. J., Bibb, M. J., and Dijkhuizen, L. (1997) *Appl. Environ. Microbiol.* **63,** 956–961
16. Thompson, J. D., Gibson, T. J., Plewniak, F., Jeanmougin, F., and Higgins, D. G. (1997) *Nucleic Acids Res.* **25,** 4876–4882
17. Redenbach, M., Kieser, H. M., Denapaite, D., Eichner, A., Cullum, J., Kinashi, H., and Hopwood, D. A. (1996) *Mol. Microbiol.* **21,** 77–96
18. Gust, B., Challis, G. L., Fowler, K., Kieser, T., and Chater, K. F. (2003) *Proc. Natl. Acad. Sci. U. S. A.* **100,** 1541–1546
19. Kieser, T., Bibb, M., Buttner, M., Chater, K., and Hopwood, D. A. (2000) *Practical Streptomyces Genetics*, pp. 408–414, The John Innes Foundation, Norwich, UK
20. Bystrykh, L. V., Fernandez-Moreno, M. A., Herrema, J. K., Malpartida, F., Hopwood, D. A., and Dijkhuizen, L. (1996) *J. Bacteriol.* **178,** 2238–2244
21. Tsao, S. W., Rudd, B. A., He, X. G., Chang, C. J., and Floss, H. G. (1985) *J. Antibiot.* **38,** 128–131
22. de Koning, W., and van Dam, K. (1992) *Anal. Biochem.* **204,** 118–123
23. Morris, D. L. (1948) *Science* **107,** 254–255
24. Christensen, B., and Nielsen, J. (1999) *Metab. Eng.* **1,** 282–290
25. Wiechert, W. (2001) *Metab. Eng.* **3,** 195–206

26. Borodina, I., Krabben, P., and Nielsen, J. (2005) *Genome Res.* **15,** 820–829
27. Davidson, A. (1992) *Quantitative Microbial Physiology of Streptomyces coelicolor A3*(2). Ph.D. thesis, University of Glasgow, Glasgow
28. Paget, M. S., Kang, J. G., Roe, J. H., and Buttner, M. J. (1998) *EMBO J.* **17,** 5776–5782
29. Vinciotti, V., Khanin, R., D'Alimonte, D., Liu, X., Cattini, N., Hotchkiss, G., Bucca, G., de Jesus, O., Rasaiyaah, J., Smith, C. P., Kellam, P., and Wit, E. (2005) *Bioinformatics* (*Oxf.*) **21,** 492–501
30. Yang, Y. H., Dudoit, S., Luu, P., and Speed, T. (2001) in *Microarrays: Optical Technologies and Informatics* (Bittner, M. L., Chen, Y., Dorsel, A. N., and Dougherty, E. R., eds) Vol. 4266, Proceedings of SPIE, San Jose, CA
31. Kerr, M. K., Martin, M., and Churchill, G. A. (2000) *J. Comput. Biol.* **7,** 819–837
32. Patil, K. R., and Nielsen, J. (2005) *Proc. Natl. Acad. Sci. U. S. A.* **102,** 2685–2689
33. Segre, D., Vitkup, D., and Church, G. M. (2002) *Proc. Natl. Acad. Sci. U. S. A.* **99,** 15112–15117
34. Patil, K. R., Rocha, I., Forster, J., and Nielsen, J. (2005) *BMC Bioinformatics* **6,** 308
35. van Keulen, G., Siebring, J., Rembacz, K. P., Hoogeveen, M., Tomczynska, M., and Dijkhuizen, L. (2004) *J. Microbiol. Methods* **58,** 139–142
36. Lessie, T. G., and Wyk, J. C. (1972) *J. Bacteriol.* **110,** 1107–1117
37. Wittmann, C., Kromer, J. O., Kiefer, P., Binz, T., and Heinzle, E. (2004) *Anal. Biochem.* **327,** 135–139
38. Heinisch, J. (1986) *Curr. Genet.* **11,** 227–234
39. Wilson, W. A., Wang, Z., and Roach, P. J. (2002) *Mol. Cell. Proteomics* **1,** 232–242
40. Bruton, C. J., Plaskitt, K. A., and Chater, K. F. (1995) *Mol. Microbiol.* **18,** 89–99
41. Karandikar, A., Sharples, G. P., and Hobbs, G. (1997) *Microbiology* **143,** 3581–3590
42. Schneider, D., Bruton, C. J., and Chater, K. F. (2000) *Mol. Gen. Genet.* **263,** 543–553
43. Meile, L., Rohr, L. M., Geissmann, T. A., Herensperger, M., and Teuber, M. (2001) *J. Bacteriol.* **183,** 2929–2936
44. Orban, J. I., and Patterson, J. A. (2000) *J. Microbiol. Methods* **40,** 221–224
45. Heath, E. C., Hurwitz, J., Horecker, B. L., and Ginsburg, A. (1958) *J. Biol. Chem.* **231,** 1009–1029
46. Lampen, J. O., Gest, H., and Sowden, J. C. (1951) *J. Bacteriol.* **61,** 97–98
47. Sonderegger, M., Schumperli, M., and Sauer, U. (2004) *Appl. Environ. Microbiol.* **70,** 2892–2897
48. Rollin, C., Morgant, V., Guyonvarch, A., and Guerquin-Kern, J. L. (1995) *Eur. J. Biochem.* **227,** 488–493
49. Hesketh, A. R., Chandra, G., Shaw, A. D., Rowland, J. J., Kell, D. B., Bibb, M. J., and Chater, K. F. (2002) *Mol. Microbiol.* **46,** 917–932
50. Natsume, R., Takeshita, R., Sugiyama, M., Ohnishi, Y., Senda, T., and Horinouchi, S. (2003) *Acta Crystallogr. Sect. D Biol. Crystallogr.* **59,** 2313–2315
51. Onaka, H., Nakagawa, T., and Horinouchi, S. (1998) *Mol. Microbiol.* **28,** 743–753
52. Stohl, E. A., Brockman, J. P., Burkle, K. L., Morimatsu, K., Kowalczykowski, S. C., and Seifert, H. S. (2003) *J. Biol. Chem.* **278,** 2278–2285
53. Sheng, D., Liu, R., Xu, Z., Singh, P., Shen, B., and Hua, Y. (2005) *DNA Repair* **4,** 671–678
54. Pages, V., Koffel-Schwartz, N., and Fuchs, R. P. (2003) *DNA Repair* **2,** 273–284
55. Galvao, C. W., Pedrosa, F. O., Souza, E. M., Yates, M. G., Chubatsu, L. S., and Steffens, M. B. (2003) *Can. J. Microbiol.* **49,** 145–150
56. Vierling, S., Weber, T., Wohlleben, W., and Muth, G. (2000) *J. Bacteriol.* **182,** 4005–4011
57. Olukoshi, E. R., and Packter, N. M. (1994) *Microbiology* **140,** 931–943
58. Olukoshi, E. R., and Packter, N. M. (1992) *Biochem. Soc. Trans.* **20,** 99
59. Packter, N. M., and Olukoshi, E. R. (1995) *Arch. Microbiol.* **164,** 420–427
60. Alper, H., Jin, Y. S., Moxley, J. F., and Stephanopoulos, G. (2005) *Metab. Eng.* **7,** 155–164
61. Alper, H., Miyaoku, K., and Stephanopoulos, G. (2005) *Nat. Biotechnol.* **23,** 612–616
62. Avignone, R., White, J., Kuiper, A., Postma, P. W., Bibb, M., and Teixeira de Mattos, M. J. (2002) *Metab. Eng.* **4,** 138–150
63. Vining, L. C. (1992) *Gene* (*Amst.*) **115,** 135–140